Density functional theory calculations of the turbostratically disordered compound [(SnSe)_{1+y}]_{m}(VSe_{2})_{n}

Sven P. Rudin and David C. Johnson

Density Functional Theory Calculations of the Turbostratically Disordered Compound $[(SnSe)_{1+y}]_m(VSe_2)_n$

Sven P. Rudin

Los Alamos National Laboratory, Los Alamos, New Mexico 87545, USA

David C. Johnson

Department of Chemistry and Materials Science Institute,

University of Oregon, Eugene, Oregon 97403, USA

(Dated: April 15, 2015)

Abstract

Among composite materials that layer constituent substances of nanoscale thicknesses, $[(SnSe)_{1+y}]_m(VSe_2)_n$ emerges as an example where the constituents retain incommensurate lattice structures. Perpendicular to the stacking direction, the system exhibits random translations and random rotations on average, i.e. turbostratic disorder, with local regions showing twelvefold diffraction patterns. Earlier theoretical work on these structures showed that combining density functional theory with an empirical treatment of the van der Waals interaction gave structural parameters in good agreement with experiment, but no attempt was made to examine the relative orientations. Here we approximate the extended system with one extended constituent and one finite constituent, which allows the treatment of all relative orientations on equal footing. The calculations show how the twelvefold periodicity follows from how the ions of the SnSe layer lock in with favored positions relative to the VSe_2 layer, and the associated energy scale supports arguments for the overall turbostratic disorder. The success of this approximation in describing the structural parameters of the extended $[(SnSe)_{1+y}]_m(VSe_2)_n$ system encourages its use for other properties and for other similar systems with other chemistries.

PACS numbers: 61.46.-w, 61.44.Fw,

I.   INTRODUCTION

Two-dimensional layers on substrates and composite materials that layer two or more constituent substances of nanoscale thickness often show interesting properties not found in the individual bulk constituents. Prominent examples include the remarkable properties of graphene,[1–3] the transition from an indirect to a direct band gap predicted for $MoSe_2$ when thinning the bulk down to a monolayer,[2,4,5] and a charge density wave transition in composites containing monolayers of VSe_2 separated by layers of $SnSe$.[6–8] A change from 3D to 2D has also been shown to lead to changes in interlayer coupling, the degree of quantum confinement and in electronic structures.[9] The intriguing properties of nanocomposites arise in many different ways: from how the constituents' properties interact,[10] from the effects of the nanoscale dimensions on the constituents,[8] or from the interface effects amplified by the nanoscale dimensions.[11,12] Understanding the source of the properties ideally leads to the ability to experimentally control them and also to the ability to predict what composites might best serve in a specific technological application.

Two aspects of the constituent materials affect the outcome of their combination: how their crystal structures compare and their structural flexibility. Interweaving layers of 2D constituents with the structural flexibility to conform, Cario and coworkers were able to predict both the structures and the compositions of ten new compounds.[13,14] For systems with less structural flexibility, however, the incompatibility can cause in-plane lattice vectors to distort to achieve commensurate axes, inducing strains which lead to interesting effects. Misfit layered compounds that alternate layers of a rock salt structured constituent with a transition metal dichalcogenide exemplify systems where the layers of the constituents coincide in one of the in-plane axes, while the other in plane axes of the two different constituents have an irrational length ratio.[15–17] In the incommensurate direction the two constituents mutually modulate each other's sublattice.[18–22] For other systems, the incompatibility is too large, their structural flexibility is too small, and the constituents retain lattice constants close to their bulk values. Examples of this type of system are layered materials with turbostratic disorder, which consist of parallel layered constituents where both the translation parallel to the layer and the rotation about the normal are on average random.[23,24] While planes of atoms may be periodic along the common c axis direction, the lack of coherence from one layer to the next means that these systems are not superlattices.

Removing the requirement of using constituents with compatible lattices increases the number of possible material combinations. This freedom widens the chances of designing a material with desired properties. The drawback of the larger number of combinations is the increased effort needed for their exploration. The disordered polytypes of the misfit layered compounds discussed above can be prepared using a kinetically controlled synthesis approach,[25] but synthesizing and characterizing them all becomes quickly too expensive. A theoretical exploration can be much quicker than experiment, but the theoretical approach must also be reliable. Density functional theory (DFT) appears to be a good choice in terms of reliability. The size of the unit cells affects the speed of the calculations and hence of the exploration. Making the size of the unit cells manageable motivates this work.

The work presented here focuses on a known system that exhibits turbostratic disorder, $[(SnSe)_{1+y}]_m(VSe_2)_n$.[6] In it, two SnSe layers alternate with Se-V-Se trilayers. The VSe_2 layer retains the layered structure found in solid VSe_2. The SnSe layer can be viewed as a distorted NaCl-type crystal, in particular with slightly different z values along the stacking direction for the Sn and Se ions (z_{Sn1}, z_{Se1}). The $1+y$ is measured around 1.15. Experiment reveals local regions with individual or superimposed twelvefold diffraction patterns, and preliminary DFT results suggest a preference for orientations with a twelvefold pattern.[26]

Earlier DFT work on $[(SnSe)_{1+y}]_m(VSe_2)_n$ structures relied on (periodic) unit cells with approximately rational ratios of the measured lattice vectors of SnSe and VSe_2 crystals.[7] Optimization with DFT of these unit cells resulted in structural parameters in good agreement with experiment. But for an exploration of combinations of constituents this approach introduces a commensurability that artificially constrains the constituents and severely limits which relative angles can be treated.

Using DFT to systematically study the effects of changing the angle between the SnSe and the VSe_2 layers requires an approach that treats all angles on an equal footing. In particular, such a study imposes three constraints on the unit cells: to have (1) in-plane lattice vectors with close to integer values of both constituent system lattices (2) for a sequence of relative angles between constituent systems (3) with reasonable numbers of atoms that can be treated with DFT. Experience shows that these three constraints cannot all be fulfilled simultaneously. To overcome this impediment, the approximation presented here leaves one constituent as a continuous layer and treats the other constituent as a finite system, i.e., as an island sandwiched between the continuous layers (see Fig. 1).
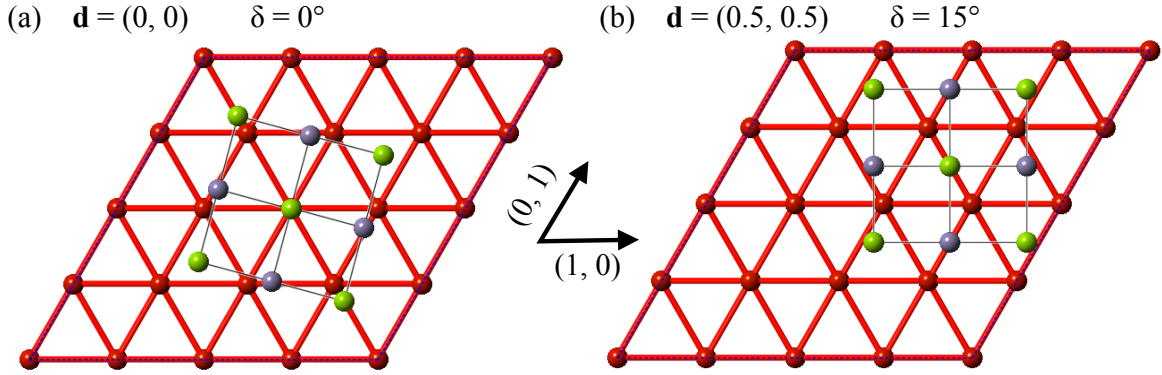
FIG. 1. (Color online) Top view of typical (a) high- and (b) low-symmetry unit cells employed in the current calculations. This current work approximates the incommensurate $[(SnSe)_{1+y}]_m(VSe_2)_n$ structures with infinite VSe_2 planes that sandwich finite SnSe islands (initially given a NaCl-like crystal structure with differing z components for Sn and Se in the stacking direction). The cell is defined in the plane by N_V^2 VSe_2 unit cells (shown in red are the V sites for a 4×4 cell). Over this lies a layer of SnSe (grey and green ions), situated with (1) an angle δ between the two layers' lattice vectors and (2) a relative in-plane offset $\mathbf{d}$ between the center of the cell and the central Se and Sn ions.

The work presented here aims to establish this approach as a reliable approximation to make dependable, DFT-based predictions for misfit layered compounds. The calculations treat only one layer of each constituent in unit cells with a well-defined relative orientation. With the current approach established, future research may study many of the interesting phenomena excluded here, including interactions across multiple layers. Section II details how we approximate one constituent as a finite system and outlines the specifics of the DFT treatment. Section III reports the results of DFT calculations that apply the approximation to the $[(SnSe)_{1+y}]_m(VSe_2)_n$ system, followed by a summary and conclusions in Sec. IV.

II. METHOD

All results presented here originate in DFT calculations using the VASP package.[27,28] The calculations make use of the generalized gradient approximation (GGA) of Perdew, Burke, and Ernzerhof,[29] and rely on a single k-point (Γ). Increasing the number of k-points changes the energies by fractions of an meV/atom and the relaxed structural parameters by

fractions of a percent, i.e., at scales well below those of interest here. Initial calculations on islands with up to 25 Sn (Se) ions use Fermi-Dirac smearing with $\sigma = 27$ meV and an energy difference of 10^{-8} as the convergence criterion; calculations on larger islands use $\sigma = 100$ meV and and an energy difference of 10^{-4}. To overcome the GGA functional's inability to correctly include the van der Waals interaction, the calculations include a pair-wise empirical approximation thereof, the DFT-D2 method of Grimme,[30] with the default values for the parameters.[31]

To accommodate the two incompatible sets of in-plane lattice vectors for any relative orientation, the calculations presented here treat one constituent as a finite system. Specifically, the calculations employ unit cells that contain (1) a continuous layer of $(N_V)^2$ VSe_2 unit cells that sandwiches (2) a finite SnSe island with N_{SnSe} Sn and N_{SnSe} Se ions. As shown below, this approximation and its adjustable parameter N_{SnSe} successfully allow for the turbostratic disorder to be explored and understood. The reverse choice with full SnSe layers sandwiching finite VSe_2 islands proves unreliable, because structural optimization severely distorts the finite VSe_2 islands. For the same reason, a treatment of both constituents as finite fails. Structural optimization distorts the SnSe islands to a very small degree.

Figure 1 shows how the constituents relate in the plane. The figure uses $N_V = 4$ and $N_{SnSe} = 9$ as an example. The SnSe islands are initially constructed from NaCl-type crystal structure unit cells, the only aspects of the experimentally-observed "distortions" included are the different z components z_{Sn1} and z_{Se1}. The relative angle δ is defined as 0° when the diagonals of both constituents' unit cells coincide. The twelve options available for choosing $\delta = 0°$ suggest an origin for the experimental observation of twelvefold diffraction patterns. The offset $\mathbf{d}$, given in units of the VSe_2 unit cell, measures the horizontal distance between the centers of each constituent. For all systems considered here, N_V is even, while the SnSe islands are all constructed symmetrically around a central pair of Sn, Se atoms (all N_{SnSe} are odd), resulting in $\mathbf{d} = (0,0)$ situating both constituents' central atoms above one another.

III. RESULTS

As shown in Ref. 7, optimization of structures with the method outlined here, but without making one of the layers finite, leads to excellent agreement between the average values of the theoretically optimized and experimentally measured (average) structural parameters. This
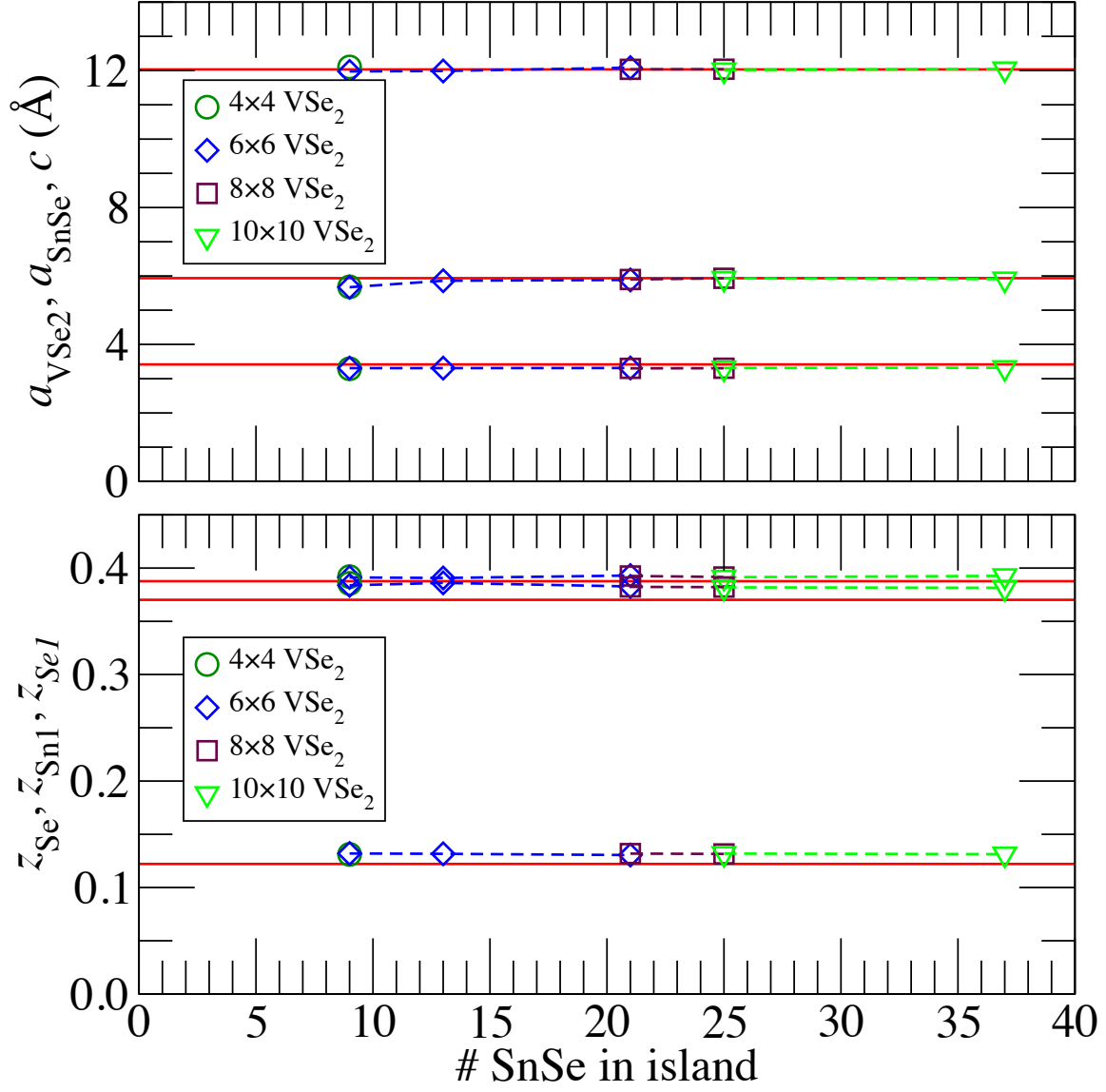
FIG. 2. (Color online) Optimized structural parameters for SnSe islands sandwiched between VSe$_2$ layers, as function of island size and for sequence of unit cell sizes given by VSe$_2$ grid. Solid horizontal lines show the experimental value. The parameters are averaged over the appropriate ions or bonds in the unit cell. Calculations optimize optimally placed initial structures ($\delta = 15°$, $\mathbf{d} = (0, 0)$), see below.

agreement also holds with one of the layers made finite, as demonstrated here by analyzing structures that were fully optimized from initial geometries with the preferred δ and $\mathbf{d}$ (see below). Structures with different initial geometries transformed upon optimization into structures with the preferred values for δ and $\mathbf{d}$. Figure 2 shows the rapid convergence

with island size of the structural parameters for fully optimized geometries. The absolute parameters (a_{VSe_2}, a_{SnSe}, c) agree very well with experiment. The calculated fractional parameters (z_{Se}, z_{Sn1}, z_{Se1}) consistently lie slightly higher than the measured values. These values measure the vertical distances from the V plane. The small error in z_{Se} suggests a slight underbonding between V and Se, possibly due to the approximate treatment of the van der Waals forces.

Results presented in the remainder of this section stem from calculations that do not optimize the structures. Performing calculations without structural optimization means the systems retain their initial, well-defined values for the angle δ and the offset $\mathbf{d}$ between the SnSe and the VSe$_2$ layers. The dependence of the results on the well-defined δ and $\mathbf{d}$ complements what experiments reveal about $[(\text{SnSe})_{1+y}]_m(\text{VSe}_2)_n$ and aids in understanding the results of measurements. To that end, we begin with the least realistic system containing the smallest possible SnSe island: a single SnSe "dimer."

Figure 3 shows the energy of a single SnSe dimer, i.e., an island with zero radius, as a function of the offset $\mathbf{d}$. The plotted energies are for unrelaxed structures with parameters as discussed at the start of this section, the angle δ for a zero-radius island being undefined. The energy surface reveals three offsets $\mathbf{d}$ with zero gradient, which mark geometries with high symmetry. The most favorable position has the dimer centered between two Se triangles (in line with a V ion). The least favorable position has the dimer centered over a V triangle with the dimer's Sn ion adjacent to (and in line with) a Se ion of the VSe$_2$ layer. The same arrangement but with the dimer's Se ion adjacent to a Se ion of the VSe$_2$ layer gives the third point on the energy surface with zero gradient at an intermediate energy. Given the ions' large coordination in solid Se and SeSn, it makes sense that the most favorable geometry here has the largest coordination number for the dimer's ions, while the least favorable position minimizes the coordination numbers. The results calculated for this system, while experimentally unrealistic, deliver the key to understanding the preferred relative orientation of the two constituent systems.

Figure 4(a) shows how the offset affects the total energy for the largest islands considered here, with 69 Sn (Se) ions, at two angles δ. For both angles the energy surfaces exhibit a wave-like structure, albeit spanning significantly different energy ranges: for $\delta = 15°$ the range is nearly a factor of seven larger than for $\delta = 0°$. At $\delta = 15°$ (and $45°$, $75°$, etc.) the lattice vectors of the SnSe layer line up with one lattice vector of the VSe$_2$ layer. Setting
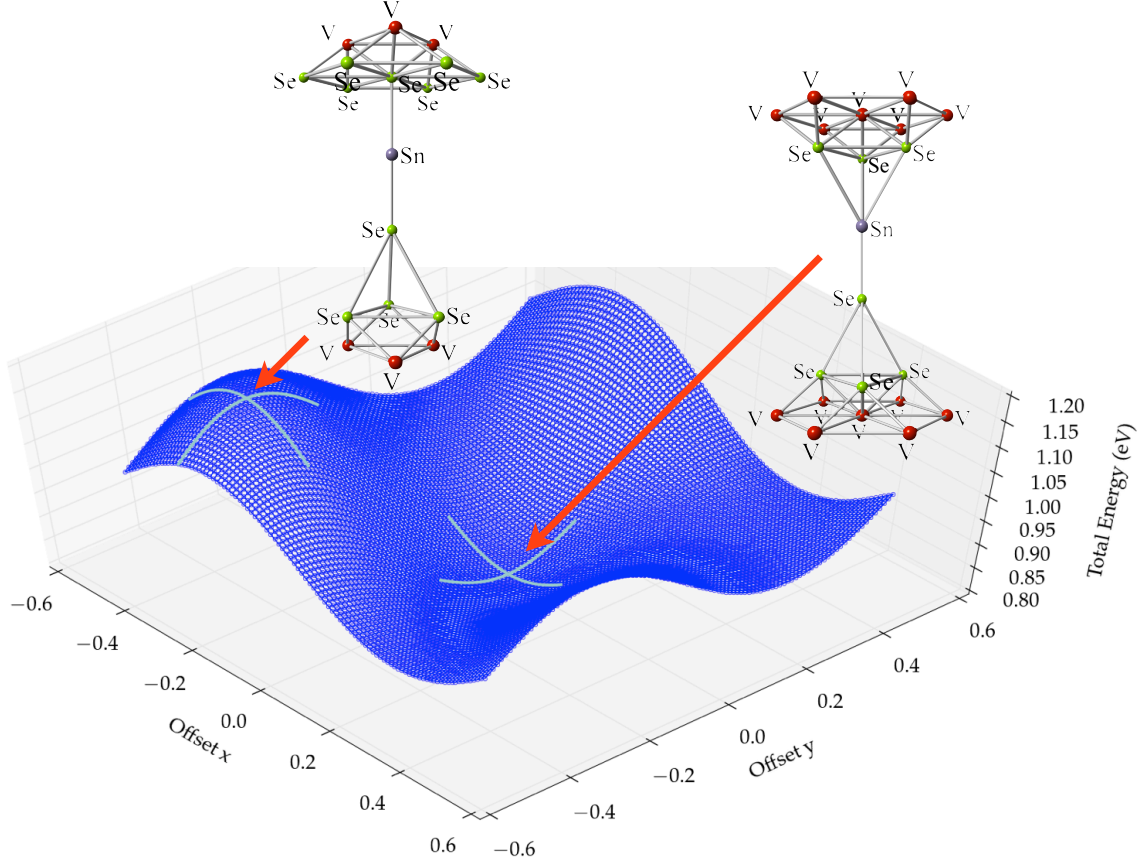
FIG. 3. (Color online) Calculated energies for SnSe "dimer" (island with zero radius) sandwiched between 4×4 VSe$_2$ layers with offsets scanned across a VSe$_2$ unit cell. Structures are not relaxed. The minimum occurs at $\mathbf{d} = (0,0)$, where the dimer sits centered over a Se triangle and inline with a V ion (inset); the maximum is at $\mathbf{d} = (-1/3, -1/3)$, where the dimer sits centered in a V triangle with the Sn ion adjacent to a Se ion (inset). The latter geometry but with the dimer's Se ion adjacent to a Se ion (not shown) occurs at $\mathbf{d} = (+1/3, +1/3)$, where the energy surface exhibits a third point with zero slope.

$\mathbf{d}_x \approx \pm 0.5$ places lines of Sn and Se ions in the unfavorable region of Fig. 3, while $\mathbf{d}_x \approx 0.0$ places them in the favorable region.

The overall difference in character between $\delta = 0°$ and $\delta = 15°$ can be understood by approximating the SnSe islands as a collection of independent SnSe dimers. For this approximation, the total energy sums the energy surface mapped out in Fig. 3 for each dimer. Figure 4(b) shows the results of such a convolution, with the system approximated as 69 independent dimer systems. The offset due to overcounting the VSe$_2$ layer remains in the
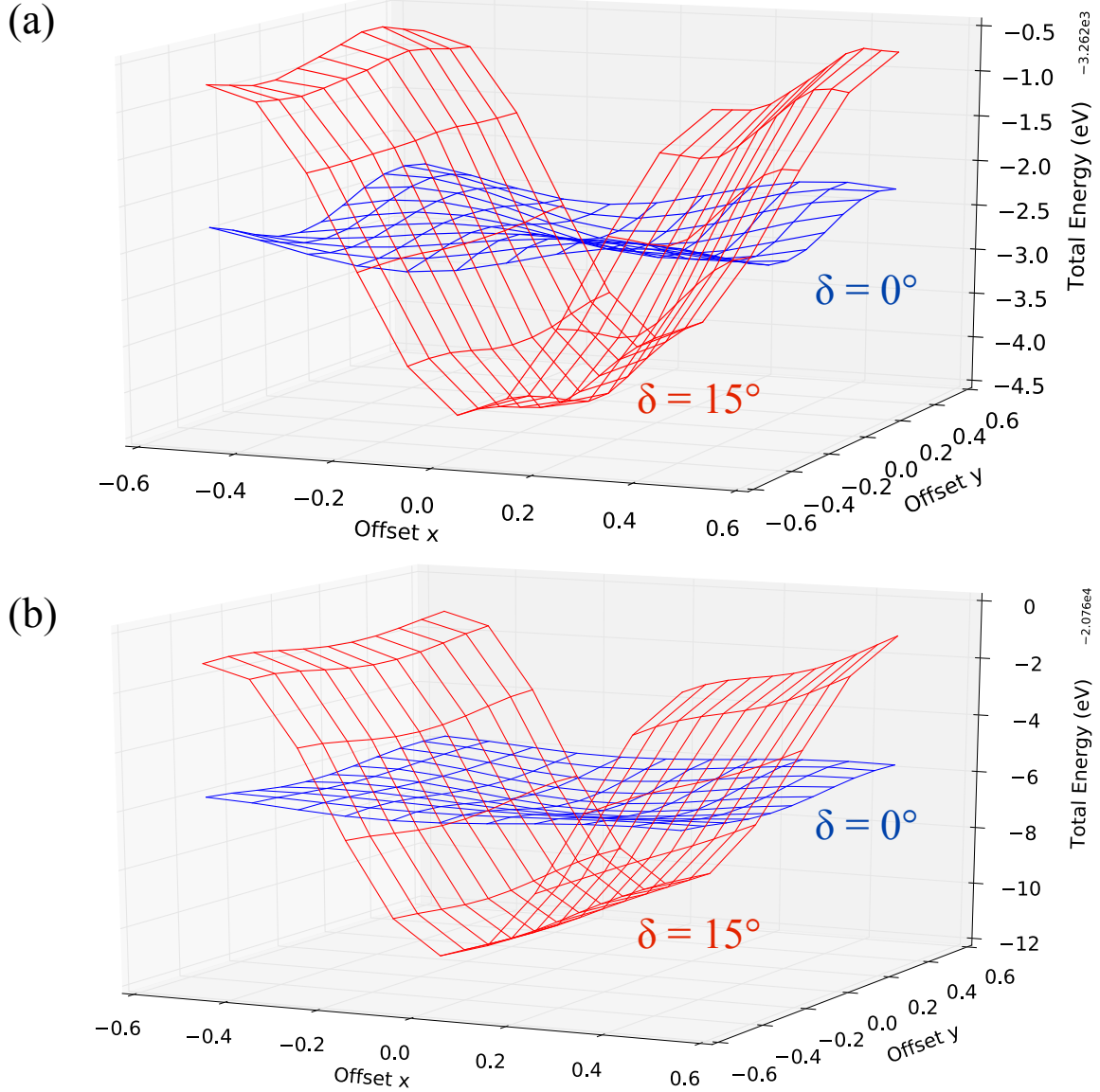
8

FIG. 4. (Color online) (a) Calculated energies for SnSe islands with 69 Sn (Se) ions sandwiched between 12×12 VSe$_2$ layers at $\delta = 0°$ (blue) and $\delta = 15°$ (red) with offsets scanned across a VSe$_2$ unit cell, and (b) energy calculated by adding the energies of 69 dimer systems (Fig. 3) with SnSe dimer located at in-plane positions of the 69 Sn (Se) ions. Structures are not relaxed.

total energy. The missing perturbations due to the bonding among the "dimers" in the island result in many differences between the energy surfaces in Fig. 4(a) and Fig. 4(b), including scale and structural details. But the approximation replicates the characteristic relative difference between maximum and minimum energies and the general shape for $\delta = 15°$.

A comparison of the calculations with a single and with 69 Sn (Se) ions in the island,

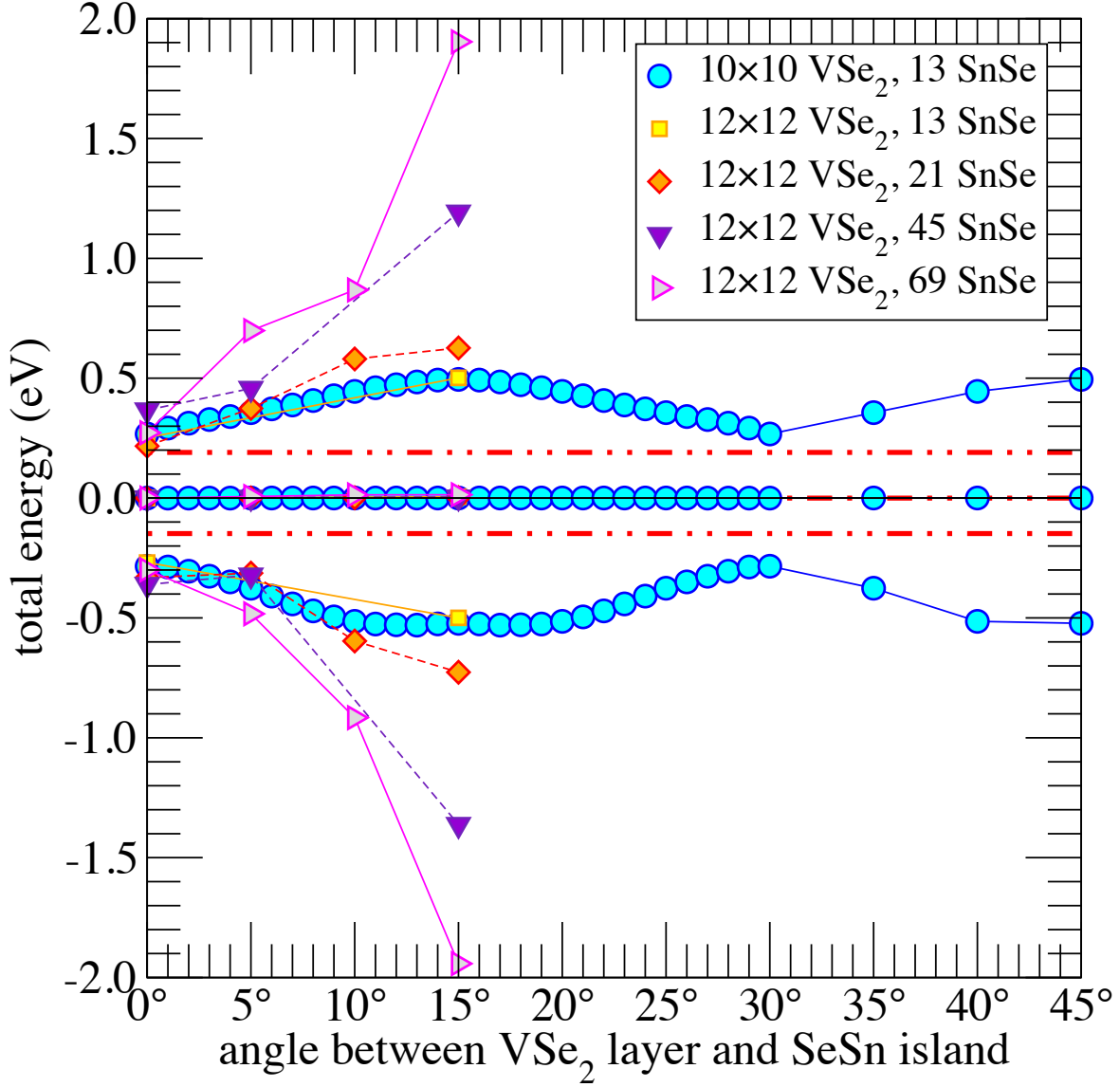FIG. 5. (Color online) Calculated average, maximum, and minimum energies of scans across **d** for SnSe islands sandwiched between VSe$_2$ layers. The structures are not relaxed. Comparison of the results for islands with 13 Sn (Se) ions calculated in unit cells with 10×10 and 12×12 VSe$_2$ at $\delta = 0°$ and $\delta = 15°$ show minor differences, but not on a scale relevant to current conclusions (both unit cells are large enough to keep periodic versions of the islands well separated).

demonstrate how increasing the island size changes the characteristics of the energy surfaces. The energy difference between favored and unfavored offset **d** increases. The shape of the energy surface for $\delta = 15°$ in particular develops an independence of the energy on one component of the offset. For the bottom of the energy valley this independence stems

from an increased number of ions that sample the energy surface in Fig. 3 along the line connecting the $\mathbf{d} = (0,0)$ minima in adjoining unit cells: once this energy cut of the surface is sufficiently well sampled, a shift of the sampling along the line has no effect.

Figure 5 shows the average, maximum, and minimum energies of scans across $\mathbf{d}$ as a function of angle. The average energy is independent of angle (on the scale shown here). The maxima and minima oscillate with a 30° periodicity. The dependence on system size of the extrema oscillates with the same periodicity; the number of ions in the island has little effect on the extrema for $\delta = 0°$, while near $\delta = 15°$ the effect becomes dramatic.

The limited effect of island size on the range exhibited by the energy surfaces at $\delta = 0°$ reveals the two constituent systems' structural incompatibility in this orientation. At $\delta = 0°$ there is no choice of $\mathbf{d}$ where the two constituents' lattice vectors can lock in. As a result, if a dimer in the SnSe island already occupies the favored $\mathbf{d}$, growing the island cannot place any additional dimer at a favorable $\mathbf{d}$. Conversely, for locked-in lattice vectors at $\delta = 15°$, increasing the size of the SnSe island places additional dimers at or near a favorable $\mathbf{d}$.

Figure 6 shows the effect of SnSe island size on calculated energy maxima and minima at $\delta = 15°$, relative to average energy. Both extrema's dependence on island size fit linear behavior very well. The energy gained by increasing island size is approximately -13 meV per ion in the island.

The results presented here suggest explanations for what is observed experimentally in the $[(\mathrm{SnSe})_{1+y}]_m(\mathrm{VSe}_2)_n$ system, which is representative of the turbostratically disordered misfit layered compounds prepared using modulated elemental reactants. The ab plane diffraction patterns for $[(\mathrm{SnSe})_{1+y}]_1(\mathrm{VSe}_2)_1$ contain independent $hk0$ reflections for both SnSe and VSe_2. While large area x-ray experiments of the ab plane show a random orientation, transmission electron nanodiffraction yields local regions with twelve-fold symmetry. This reflects the preference for such orientations found and explained here.

The energy scales at work explain the overall turbostratic disorder during the self-assembly process. If the whole sample were grown dimer by dimer then the twelve-fold symmetry would prevail. But it is believed that the sample grows by a combination of nucleation of the amorphous precursor at new sites and self-assembly of new layers that template off existing crystalline regions. The different nucleation sites are rotationally randomly orientated and connect into a map of grains with not necessarily compatible or aligned grain boundaries. The energy gained by adding to a grain a dimer with the correct orien-
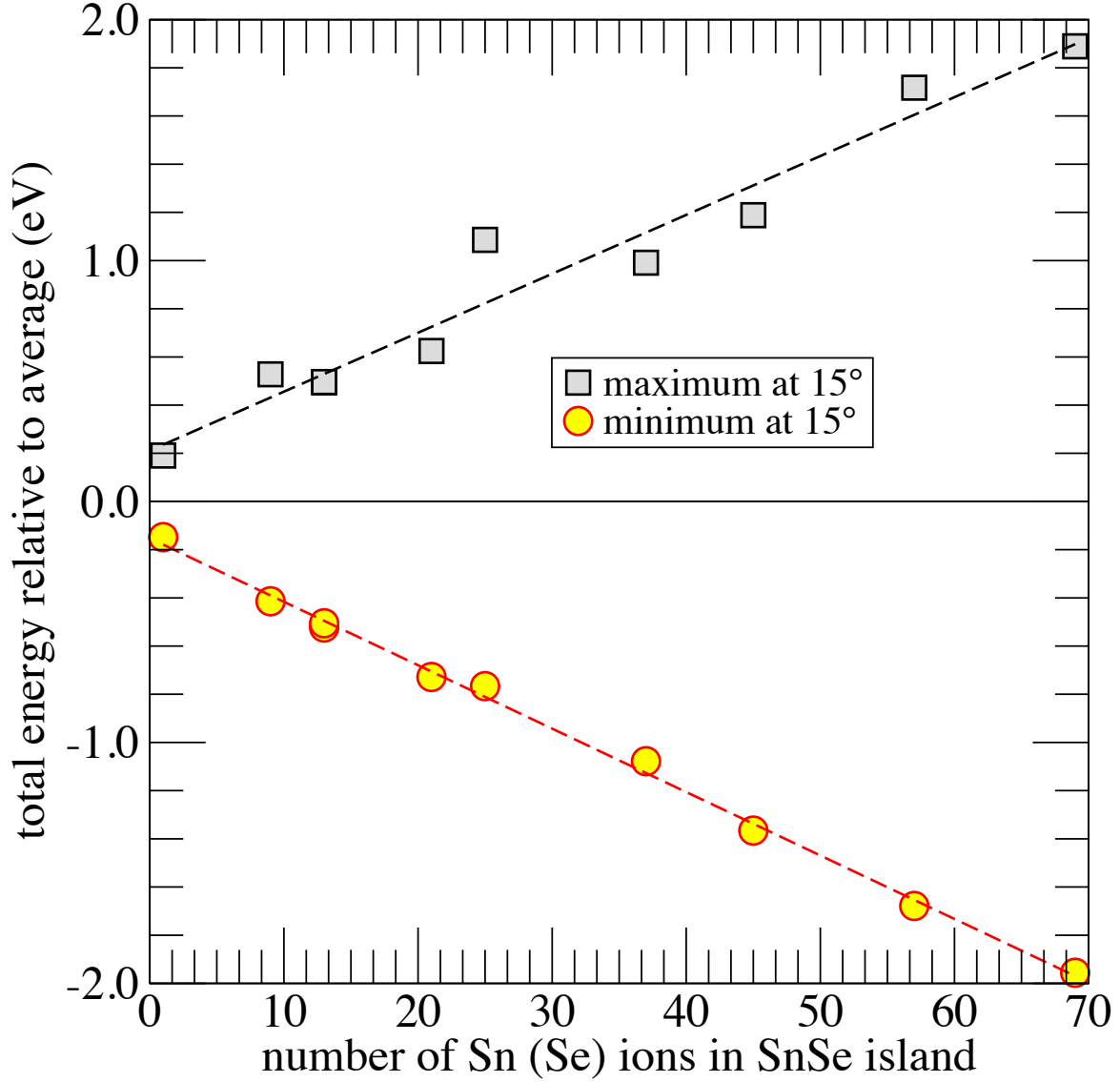
FIG. 6. (Color online) Calculated energy maxima and minima at $\delta = 15°$, relative to average energy, for SnSe islands sandwiched between VSe$_2$ layers. The structures are not relaxed. The dashed lines represent linear fits with slopes of $+24$ meV/dimer and -26 meV/dimer.

tation is small compared to room temperature, whereas the energy needed for concerted rearrangements tend to be large, making such rearrangements unlikely.

IV.   SUMMARY AND CONCLUSIONS

Earlier work on $[(SnSe)_{1+y}]_m(VSe_2)_n$ structures showed that combining DFT with the DFT-D2 method gave structural parameters in good agreement with experiment. The two constituent materials exhibit incommensurate lattice vectors, which were accommodated by finding specific relative orientations in which multiples of them matched relative well. Despite the good agreement with experiment, this approach is somewhat constraining, in particular its limitation to only specific relative orientations.

Here we approximate the extended system with one extended constituent (the VSe_2 layer) and one finite constituent (the SnSe layer), which allows the treatment of all relative orientations on equal footing. The introduced edge effects are relatively minimal, and the structural parameters converge quickly with island size. In addition, the limit of only single Sn and Se ions in the island, a SnSe dimer, reveals a distinct preference in offset relative to the VSe_2 ions, which benefits the understanding of the extended system.

The effect of relative orientation between the constituents reveals itself by studying systems that are not structurally optimized. This allows scans across the two parameters that describe the relative orientation, the angle δ and the offset $\mathbf{d}$. The results show a $30°$ periodicity in δ, i.e., the same twelve-fold symmetry observed in transmission electron nanodiffraction measurements.

The periodicity follows from how the SnSe dimers lock in with their individual favorable offset relative to the VSe_2 layer. A single dimer's most favorable offset places it centered over a Se triangle and inline with a V ion. Aligning one lattice vector of SnSe dimers with a line of V ions maximizes the number of dimers situated over a V ion. The twelve choices for this alignment generate the twelve-fold symmetry.

The success of the approximation with one finite constituent in describing the structural parameters of the extended $[(SnSe)_{1+y}]_m(VSe_2)_n$ system encourages its use for other chemistries and for other properties. Transferability to other systems and other properties is not guaranteed. In particular, it is not (yet) clear whether optimization of the approximate structures will always leave the finite constituent's structure reasonably intact for binaries other than SnSe. Nonetheless, the fact that the unrelaxed structures give a reasonable approximation of the relaxed system is encouraging: it supports a materials design process that can proceed much more quickly because it does not require structural optimization.

---

[1] K. S. Novoselov, A. K. Geim, S. V. Morozov, D. Jiang, Y. Zhang, S. V. Dubonos, I. V. Grigorieva, and A. A. Firsov, Science **306**, 666 (2004), http://www.sciencemag.org/content/306/5696/666.full.pdf.

[2] RadisavljevicB., RadenovicA., BrivioJ., GiacomettiV., and KisA., Nat Nano **6**, 147 (2011).

[3] N. Staley, J. Wu, P. Eklund, Y. Liu, L. Li, and Z. Xu, Phys. Rev. B **80**, 184505 (2009).

[4] L. Yang, X. Cui, J. Zhang, K. Wang, M. Shen, S. Zeng, S. A. Dayeh, L. Feng, and B. Xiang, Sci. Rep. **4** (2014).

[5] A. Splendiani, L. Sun, Y. Zhang, T. Li, J. Kim, C.-Y. Chim, G. Galli, and F. Wang, Nano Letters **10**, 1271 (2010), pMID: 20229981, http://dx.doi.org/10.1021/nl903868w.

[6] R. Atkins, S. Disch, Z. Jones, I. Haeusler, C. Grosse, S. F. Fischer, W. Neumann, P. Zschack, and D. C. Johnson, Journal of Solid State Chemistry **202**, 128 (2013).

[7] R. Atkins, M. Dolgos, A. Fiedler, C. Grosse, S. F. Fischer, S. P. Rudin, and D. C. Johnson, Chemistry of Materials **26**, 2862 (2014).

[8] M. Falmbigl, A. Fiedler, R. E. Atkins, S. F. Fischer, and D. C. Johnson, Nano Letters **15**, 943 (2015), pMID: 25546501, http://dx.doi.org/10.1021/nl503708j.

[9] M. Chhowalla, H. S. Shin, G. Eda, L.-J. Li, K. P. Loh, and H. Zhang, Nat Chem **5**, 263 (2013).

[10] M. B. Alemayehu, G. Mitchson, J. Ditto, B. E. Hanken, M. Asta, and D. C. Johnson, Chemistry of Materials **26**, 1859 (2014), http://dx.doi.org/10.1021/cm404018a.

[11] D. B. Moore, M. Beekman, S. Disch, P. Zschack, I. Häusler, W. Neumann, and D. C. Johnson, Chemistry of Materials **25**, 2404 (2013), http://dx.doi.org/10.1021/cm400090f.

[12] N. Giang, Q. Xu, Y. Hor, A. Williams, S. Dutton, H. Zandbergen, and R. Cava, Phys. Rev. B **82**, 024503 (2010).

[13] L. Cario, H. Kabbour, and A. Meerschaut, Chemistry of Materials **17**, 234 (2005), http://dx.doi.org/10.1021/cm048180p.

[14] H. Kabbour, L. Cario, and F. Boucher, J. Mater. Chem. **15**, 3525 (2005).

[15] J. Brandt, L. Kipp, M. Skibowski, E. Krasovskii, W. Schattke, E. Spiecker, C. Dieker, and

W. Jäger, Surface Science **532–535**, 705 (2003).

[16] A. Meerschaut, ed., *Incommensurate Layered Compounds* (Mater. Sci. Forum 100–101, 1992).

[17] G. A. Wiegers, A. Meetsma, J. L. de Boer, S. van Smaalen, and R. J. Haange, Journal of Physics: Condensed Matter **3**, 2603 (1991).

[18] K. Kato and M. Onoda, Acta Crystallographica Section A **47**, 55 (1991).

[19] K. Kato and M. Onoda, Acta Crystallographica Section A **47**, 448 (1991).

[20] S. van Smaalen, Phys. Rev. B **43**, 11330 (1991).

[21] S. van Smaalen, Journal of Physics: Condensed Matter **3**, 1247 (1991).

[22] A. Yamamoto, Acta Crystallographica Section A **48**, 476 (1992).

[23] B. E. Warren, Phys. Rev. **59**, 693 (1941).

[24] J. Biscoe and B. E. Warren, Journal of Applied Physics **13**, 364 (1942).

[25] M. B. Alemayehu, M. Falmbigl, C. Grosse, K. Ta, S. F. Fischer, and D. C. Johnson, Journal of Alloys and Compounds **619**, 861 (2015).

[26] I. Häusler, R. Atkins, M. Falmbigl, S. P. Rudin, W. Neumann, and D. C. Johnson, Zeitschrift für Kristallographie - Crystalline Materials **230**, 45 (2014).

[27] G. Kresse and J. Furthmuller, Phys. Rev. B **54**, 11169 (1996).

[28] G. Kresse and D. Joubert, Phys. Rev. B **59**, 1758 (1999).

[29] J. P. Perdew, K. Burke, and M. Ernzerhof, Phys. Rev. Lett. **77**, 3865 (1996).

[30] S. Grimme, Journal of Computational Chemistry **27**, 1787 (2006).

[31] The parameters for Grimme's potential are: $C_6 = 12.64$ Jnm^6/mol, $R_0 = 1.771$ Å for Se; $C_6 = 38.71$ Jnm^6/mol, $R_0 = 1.804$ Å for Sn; $C_6 = 10.80$ Jnm^6/mol, $R_0 = 1.562$ Å for V.